THE ASTROPHYSICAL JOURNAL, 278:649–662, 1984 March 15

HIGH-RESOLUTION *IUE* OBSERVATIONS OF INTERSTELLAR ABSORPTION LINES IN THE VELA SUPERNOVA REMNANT

EDWARD B. JENKINS
Princeton University Observatory
GEORGE WALLERSTEIN
University of Washington
AND
JOSEPH SILK
University of California, Berkeley
Received 1983 May 23; accepted 1983 August 25

ABSTRACT

Ultraviolet spectra of 45 stars in the vicinity of the Vela supernova remnant were recorded by the short-wavelength echelle spectrograph aboard the *International Ultraviolet Explorer* (*IUE*). Over one-third of the stars show interstellar absorption lines at large radial velocities ($|v_{LSR}| > 60$ km s^{-1}). The mapping of these high-velocity components in the sky suggests the motions are chaotic, rather than from a coherent expansion of the remnant material. In accord with earlier conclusions from *Copernicus* data, the gas at high velocity exhibits higher than normal ionization and shows substantially less depletion of nonvolatile elements than normal interstellar material at low velocities. Relatively strong lines from neutral carbon in the two excited fine-structure states indicate that the neutral clouds within the remnant have had their pressures enhanced by the passage of the blast wave from the supernova. Also, the remnant seems to show a significant enhancement in the abundances of low-velocity Si IV, C IV, and N V over those found in the general interstellar medium.

Subject headings: interstellar: abundances — interstellar: matter — nebulae: individual — nebulae: supernova remnants — ultraviolet: spectra

I. INTRODUCTION

The Vela supernova remnant is the most favorable such object to study by means of its line absorptions as seen against background stars. In our earlier work (Jenkins, Silk, and Wallerstein 1976*a*, hereafter JSW) we studied lines of sight toward four stars in the vicinity of this remnant using ultraviolet spectra from the *Copernicus* satellite. We demonstrated that the remnant interacted with a highly inhomogeneous interstellar medium (Jenkins, Silk, and Wallerstein 1976*b*). Four high-velocity clouds were intercepted, two of which were studied in detail. The high-velocity clouds were found to show abnormal ionization, indicative of shocking rather than the usual radiative ionization. Also, they had element abundance ratios that were more like solar ratios than the usually depleted interstellar abundances. These abundances indicated that the sputtering of grains in the shocked clouds had released refractory substances into the interstellar gas; such elements are normally locked up in solid form when low-velocity quiescent gas and grains approach chemical equilibrium.

With the *IUE* satellite it is now possible to observe the spectra of stars about three magnitudes fainter than could be readily studied with *Copernicus*. This has made it possible to survey a large number of stars behind, within, and just outside the Vela remnant. The high-resolution mode of *IUE* provides somewhat less than 30 km s^{-1} resolution as compared with 15 km s^{-1} provided by *Copernicus*. The wavelength range of *IUE* extends from about 1200 to 2000 Å for the SWP camera, while the *Copernicus* scans covered selected wavelength intervals between about 1000 and 1400 Å. Hence, in this study we have surveyed many more stars, but at the sacrifice of important lines such as those of O VI, S IV, and S III. We have also found that the limiting resolution in the presence of noise for absorption lines on a single *IUE* exposure ranges from 40 to 60 km s^{-1}, rather than the nominal 30 km s^{-1} which appears to be more realistic for optimally exposed emission lines.

Spectra of 45 stars in the field of the Vela remnant were obtained with the SWP camera in high dispersion mode during three observing sessions in 1979 June, 1979 September, and 1981 June. Eight of the stars appear to lie outside the nebula's filaments and three, whose nominal distances are less than 300 pc, are likely to be foreground stars. During the first two runs the small aperture was used, and during the last run the large aperture was used. For large-aperture observations a guide star was always found, and there was no evidence of reduced resolution in this observing mode. A number of stars were observed twice to improve the signal-to-noise ratio, especially when the presence of high-velocity gas was uncertain on the basis of the first exposure. Four exposures were obtained for one star, HD 72350, because of the strong lines arising from excited fine-structure levels of C I (Jenkins *et al.* 1981, hereafter JSWL). Except for HD 72350, for which we stacked the spectra, each spectrum was measured separately, and mean velocities and equivalent widths were used.

Seven of our stars appear to be members of the galactic cluster IC 2395 (Lyngå 1962; Eggen 1982) which lies behind the southern edge of the Vela remnant. HD 74455 might be a cluster member, although its spectroscopic parallax indicates that it lies in front of IC 2395.

TABLE 1

RADIAL VELOCITIES FOR VARIOUS FEATURES TOWARD STARS WITHIN AND NEAR THE VELA REMNANT

STAR (HD)[a]	SPECTRAL TYPE	l	b	D (pc)	V_{radial} (km s^{-1}, LSR) C I	S II	Si II + Fe II	Al III	C IV + Si IV	NOTES[b]
63578	B1 IV	260.25	−10.56	390	+9	+7	+2	+19	...	1
69404	B3 Vnne	262.58	−6.46	440	+8	+14	+6	...	...	1
69973	B5 Vn	264.01	−6.90	600	...	+5	+4	...	+4	1
70309	B3 V	264.41	−6.81	390	...	−1	−7	0	+5	1
70930	B2 III	264.98	−6.50	460	+13	0	0	+8	+15	1
71459	B4 V	260.10	−2.40	320	+18:	+15	+14	+20	...	
72014	B3 Vnne	260.77	−2.20	340	...	+21	+14	+16	+36, +132:	
72067	B3 V	262.08	−3.08	680	...	+5	+3	...	...	
72088	B3 III	262.67	−3.50	680	+9	+1	0	...	+9, +94	2
72089	B5 III	263.21	−3.89	1100:	...	+8, +98	+8, +85	−2	+15	2
72127A	B3 III	262.57	−3.36	710	−2	+5	0	...	+23	
72127B	...	262.57	−3.36	710	+8:	+4	+4	+14	+20, −40, −100:	2
72179	B5 V	262.08	−2.97	680	+7	+10	+8	+16	+24	
72230	B9.5 V	262.63	−3.31	500:	+4:	+9	+2	+24	...	
72232	B7 IV	263.91	−4.26	240	+8	+7	+8	+8:	...	
72350	B5 IV	262.71	−3.19	560	+12	+9	+6	+8	+11, −117	3
72537	B3 V	263.65	−3.68	390	+10:	−5	−9	...	...	
72555	B4 V	264.84	−4.53	690	...	−1	0	...	−33:, +12:	
72648	B2 II	262.23	−2.48	1230	+19	+16	+17	+4	+12, −39	
72798	B5 III	263.77	−3.46	580	−3	+6	+5	+6	+10, +103	2
72997	B2 V	262.91	−2.58	690	+9	+9	+8	...	+7	
73010	B5 V	263.80	−3.23	500	−4	+3	−1	+3	+9, −101:	
73658	B1 II	264.68	−3.13	2400	+8	+5	0, −109	+10	+14, −37, −123:	2
74194	O9	264.04	−1.95	3100	+8	+8, −71	+8, −60	−3	+23, −37:	
74234	B2 V	266.56	−3.87	760	+15	+4	0, +64	−6	+5, −51	2, 4
74251	B5 V	266.45	−3.76	620	+7	+1	−2	−8	+9	4
74273	B2 Vn	267.13	−4.27	510	...	+4	+3	−3	+9, +156, −150:	
74319	B5 V	264.07	−1.80	520	+6	−3	−8	−4	−5, −73	2
74371	B5 Iab	264.44	−2.01	1500	...	...	...	...	+5	
74436	B5 V	266.70	−3.72	750	+13	+10	+6, −125	...	+16	4
74455	B1.5 V	266.60	−3.61	420	+4	+6	−1, −175, +96	−5	+9, −80:, −175	2
74530	B3 V	266.61	−3.54	1150	+13	−1	0, −126	0	+5, −130	4
74531	B2 IV	266.68	−3.61	900	+1	+2	−2, −134, +72	...	−1, −100	4
74580	B4 V	266.68	−3.56	600	+4	+1	+1	...	−2	2, 4
74620	B5 V	266.35	−3.25	890	+4	0	+2	−6	+3	
74662	B5 V	266.90	−3.63	910	+6	+7	+15	+5	+8, −101	4
74711	B0.5 V	265.73	−2.61	1480	+8	+17:	+7	+7	+5, +101	
74753	B0 V	268.11	−4.49	710	...	0	−7:	−4	+9	1
74773	B3 IV	266.02	−2.76	720	+8	+7	+6	+2	+7, +86	2
74920	O8	265.29	−1.95	1580	+5	0	0	...	−47, +10	2
75129	B7 II	266.59	−2.74	680	...	...	...	...	+9	
75309	B2 V	265.86	−1.90	2630	+5	+9	+10	+5	+17:	
75549	B3 V	263.94	+0.01	500	+8	−1	−7	−7	−3:	1, 2
75821	O9.5 II	266.25	−1.54	980	...	+8	+6, −90	...	+12, −90	
76161	B6 Vn	267.89	−2.43	270	...	−3	−7	...	...	1, 2

[a] NOTES ON INDIVIDUAL STARS.—

69404: C II shows a velocity of 0 km s^{-1}.
Al II shows a velocity of +17 km s^{-1}.
Ca II showed partially resolved components at +1 and +13 km s^{-1}.

72067: The observed lines are probably blends of the two components seen in Ca II.

72088: λ1608 yields −9 km s^{-1} while λ1808 yields +9 km s^{-1}.

72089: Optical spectra show six components (see Table 8). A component at −68 km s^{-1} is best seen in O I and Al II.

72127A: At Ca II six components are seen.

72127B: At Ca II three components are seen.

72179: The stellar lines are sharp.

72230: High background counts due to long exposure.

72648: The lines of C I* and C I** are extremely strong as in HD 72350 (JSWL). Both O I* and O I** are also present. The stellar lines are moderately strong and may be responsible for the discrepant velocity of Al III.

72798: All low-velocity lines may be partly stellar.

72997: C IV may be stellar.

74234: The component at +64 km s^{-1} is most clearly seen in C II.

74319: Interstellar lines are broad and their velocities scatter indicating that we are observing two blended components.

74371: Stellar lines are sharp. Only C IV is likely to be interstellar.

74436: The component at −125 km s^{-1} is most clearly seen in C II.

74530: The component at −106 km s^{-1} most clearly seen in C II.

74531: The component at −134 km s^{-1} is most clearly seen in C II.

74580: A component near −90 km s^{-1} is possibly present in O I, Si II, and C II.

74753: The interstellar lines of Fe II and Si II are surprisingly weak.

74920: Ca II shows three components.

75129: Stellar lines are sharp. Only C IV is likely to be interstellar.

75549: Interstellar Si IV is stronger than C IV. λ1608 shows −12 km s^{-1} while λ1808 shows +5 km s^{-1}.

75821: Ca II shows four components. The high velocity component is near −85 km s^{-1} for C II, Al II, and O I.

[b] NOTES.—(1) Outside the Vela Remnant. (2) Two spectra are available. (3) Four spectra are available. (4) Member of IC 2395.

II. KINEMATICS OF CLOUDS

a) Basic Data

Table 1 lists the kinematic information for our absorption lines. The observed radial velocities were corrected for Earth and spacecraft orbital motions, as well as variations in instrument temperature, and are expressed relative to the local standard of rest (LSR). For each star we list the galactic coordinates and the distances as determined by photometry and spectral type from a number of sources, with preference given to data in Eggen (1982) when available. Rather than list the velocities for all species, we have used C I to represent the lowest state of ionization, S II to represent the usually undepleted species, Si II and Fe II to represent depleted species, Al III as our only doubly ionized example, and C IV plus Si IV for triply ionized gas. The singly ionized state is most common for ordinary H I regions. A colon after a velocity means that the existence of the component is uncertain. The kinematics are further described by numerous essential notes, since the data in Table 1 have been considerably consolidated.

For a number of stars, the high-velocity component is best seen in the intrinsically strong lines of C II, rather than Fe II or Si II, but in many cases strong stellar C II features make the interstellar component of C II difficult to measure. For some stars that show sharp stellar lines but are sufficiently cool that stellar C IV and Si IV are not likely to be present, we list those ions as interstellar while omitting the less ionized species from the table.

The random errors of the velocity measurements are probably about 5 km s^{-1}, which is similar to the systematic errors. Since most of the low-velocity components lie near small positive velocity (LSR), which is to be expected in this quadrant of the Galaxy, we believe that our estimate of around 5 km s^{-1} for the total error is valid.

It is interesting to compare the velocity data in Table 1 with those in Table 3 of Wallerstein, Jenkins, and Silk (1980) for two stars in common, HD 63578 and HD 72127A. The former star showed three components, sometimes blended when the lines were too strong, at -10, $+2$, and $+18$ km s^{-1}; the first of these may be further resolved into components at -7 and -22 km s^{-1}. Our *IUE* data show that Al III at $+19$ km s^{-1} is clearly associated with the $+18$ km s^{-1} component seen with *Copernicus*, while our substantial C I, S II, and Si II lines have contributions from the $+2$ km s^{-1} feature and perhaps one of the negative velocity features. For HD 72127A, whose interstellar spectrum seems to be variable (Hobbs, Wallerstein, and Hu 1982), the low ionization features appear to be associated with the *Copernicus* features seen at -5 and $+11$ km s^{-1}, while C IV fits the component near $+24$ km s^{-1} or is a blend of the three most positive velocities as seen best in Ca II. No discrete *IUE* feature can be clearly assigned to the Ca II component at -30 km s^{-1} even though it was the second strongest Ca II line in 1977 and was the strongest in 1981 (Hobbs, Wallerstein, and Hu 1982). We note all these details not because they serve as the basis for profound conclusions, but as a warning of how much may be missed from spectra with a resolution in the 30–60 km s^{-1} range.

An inspection of Table 1 and its notes reveals the following qualitative properties of the absorbing clouds in the direction of the remnant.

1. High-velocity C I is never seen, probably due to collisional ionization in high-velocity clouds. High-velocity O I is seen only in HD 74455 (from *Copernicus* spectra) and HD 72089.
2. High-velocity S II is rare, due probably to the low f-values of the accessible lines at 1250, 1253, and 1259 Å.
3. High-velocity Si II and Fe II are most evident in stars belonging to IC 2395.
4. High-velocity Al III is never seen.

b) Velocity Distributions

The velocity distribution of triply ionized gas is probably representative of the kinematics of the Vela remnant since gas at such a high ionization is not commonly seen in the general interstellar medium, though some components due to foreground and background H II clouds in the Gum nebula may contribute, especially at low velocities (Reynolds 1976; Hippelein and Weinberger 1975). We show the velocity distribution in Figure 1, where all but the lowest velocity bins are 20 km s^{-1} wide. The velocity distribution for singly ionized clouds is only shown for $|v| > 60$ km s^{-1} because smaller velocities may be lost by blending. Uncertain components are given half-weight.

The mean velocity of the singly ionized components with $|v| > 60$ km s^{-1} is 92 ± 9 km s^{-1}, while that of the triply ionized components is 107 ± 7 km s^{-1} which is not a significant difference. Above $|v| = 60$ km s^{-1} it appears that there are as many singly ionized as triply ionized high-velocity clouds and that both velocity distributions are flat. We suggest that both types of clouds have a common origin and that the singly ionized gas has had more time to recombine. Recombination times in the range of approximately 100–5000 years for high-velocity clouds were computed by JSW using densities derived from fine-structure level populations. The fact that these times are much smaller than the age of the remnant supports our interpretation that there will be clouds which have recombined to varying degrees.

The distribution of velocities of triply ionized gas appears to consist of two components: a low-velocity component with about 10 km s^{-1} dispersion and a high-velocity component

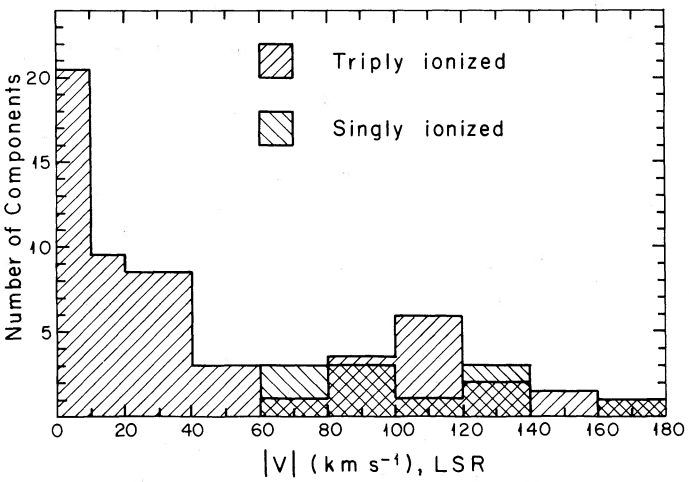

FIG. 1.—Distribution of radial velocity deviations (from the local standard of rest) for resolvable absorption-line components seen toward the Vela SNR. We are unable to plot the frequency of singly-ionized components at low velocities because they are strong and overlapping in many lines of sight.

contributing clouds with radial velocities in the range of 60–180 km s^{-1}. The high-velocity clouds have probably not interacted with the intercloud medium sufficiently to be decelerated appreciably after they were shocked. Their velocities should be inversely proportional to the square root of their preshock densities, as expected from the theory of recently shocked clouds, rather than belonging to a single Gaussian distribution, as expected for equipartition.

c) *Mapping the Velocities in l and b*

In Figure 2 we show a map of the Vela remnant region, giving the location of each observed star and the radial velocities of components seen in different stages of ionization, ranging from neutral atoms at the top to triply ionized gas at the bottom. This figure also shows a rough outline of the remnant as defined by recent soft X-ray observations by Kahn and Seward (1982).[1] Since we did not endeavor to survey the region completely, but rather to concentrate on certain areas, the coverage is neither complete nor uniform. Nevertheless a

[1] Culhane (1977) also shows a soft X-ray map of Vela, but unfortunately no coordinates are given (also, we think the picture is a reverse presentation). We used this map to check for any apparent absence of X-rays in the map of Kahn and Seward (1982) caused by incompletenesses in observing or data reduction. The Kahn and Seward map was only in preliminary form when we obtained it.

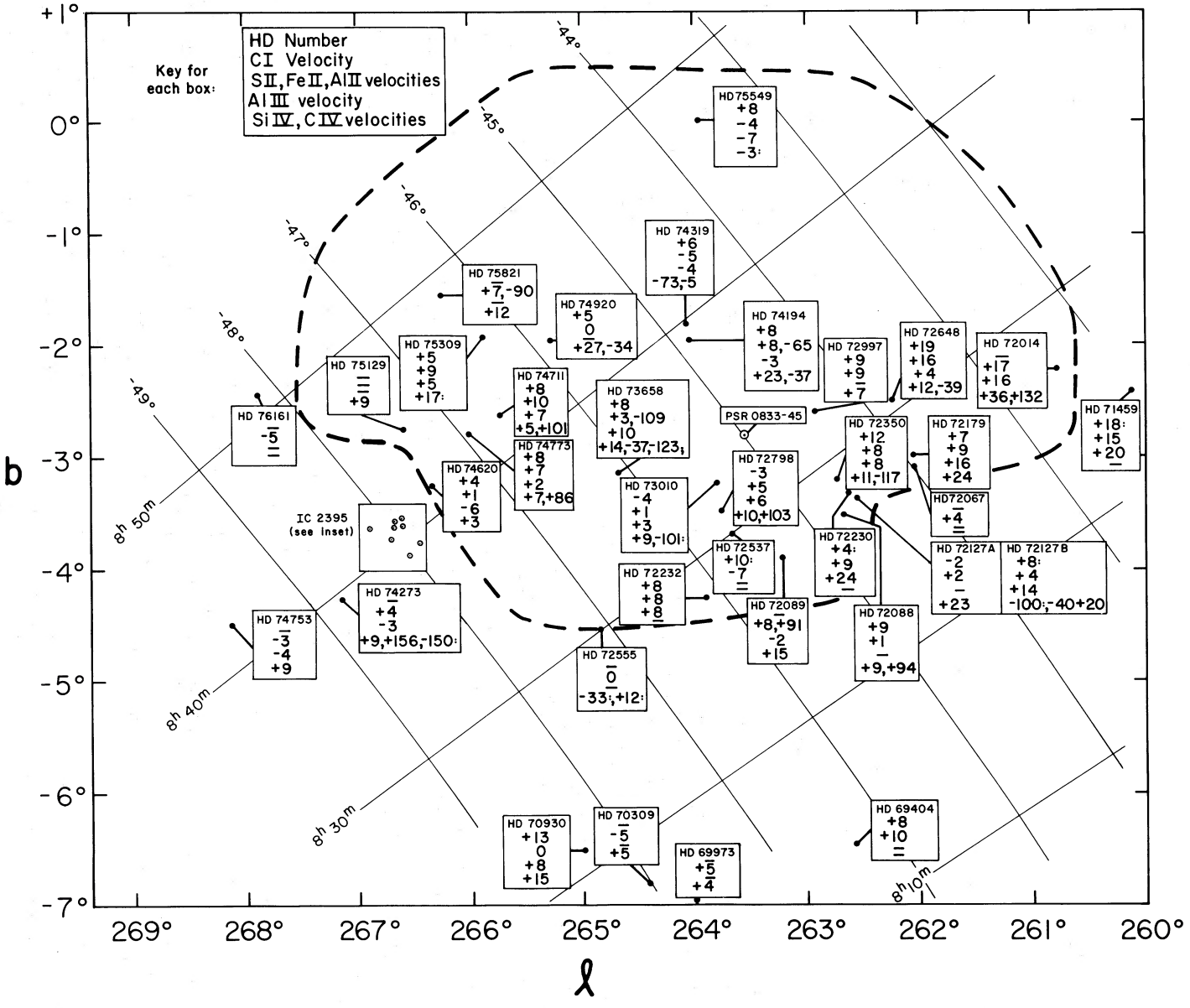

FIG. 2*a*

FIG. 2.—(*a*) Positions of stars (abscissae: galactic longitudes; ordinates: galactic latitudes) with radial velocities (LSR) of components whose ionization ranges from zero to three-times ionized. The perimeter of X-ray emission from shocked gas in the remnant is indicated by a dashed line. (*b*) Same information as in *a*), but an expanded view for a tightly packed group of stars in IC 2395.

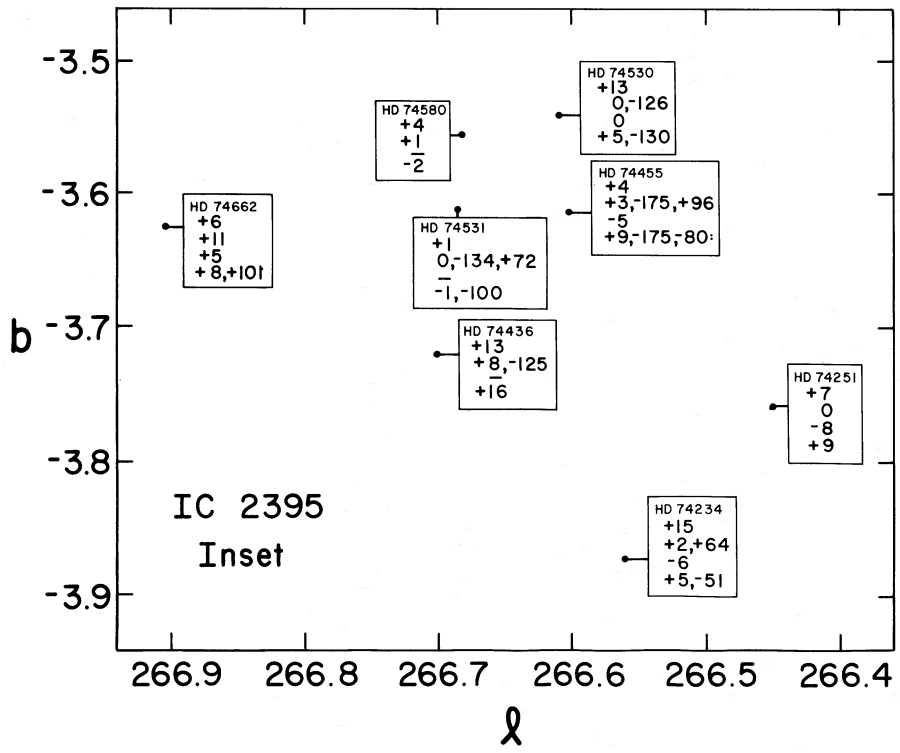

FIG. 2*b*

number of conclusions regarding the distribution of high-velocity gas can be reached by examination of Figure 2.

First, we note that all lines of sight *well outside* the remnant (i.e., HD 69404, HD 69973, HD 70309, HD 70930, and HD 74753) show no high-velocity gas. This is consistent with the absence of high-velocity gas in the Gum nebula (Wallerstein, Jenkins, and Silk 1980). Secondly, the overall behavior of the velocities seems chaotic; we see no grand design or any correlation of radial velocity with distance from either the Vela pulsar or the center of the remnant. While the high-velocity interstellar lines are almost certainly formed in shock-accelerated clouds rather than behind a shock expanding into a uniform medium, we still expect that the material will be moving predominantly radially from the explosion epicenter and thus would show higher projected radial velocities near the center, rather than the periphery, of the remnant. But to the contrary, we found high-velocity components in six of the eight stars in IC 2395, located about 3° from the remnant's center in a region where there are virtually no filaments (see Fig. 1 of JSW) or soft X-ray emission. Also, two other outlying stars, HD 74273 and HD 72014, show high-velocity, triply ionized components.

McKee, Cowie, and Ostriker (1978) have calculated the acceleration of clouds by the steady flow of intercloud material behind a remnant's blast wave. Their results indicated that at various distances out from the remnant's center there should be a complicated mixture of rapidly and slowly moving material. Some of the high-velocity clouds near (and even beyond) the blast wave originated from near the center of the remnant where the ram pressures were once very high. These clouds should now be overtaking the more recently shocked clouds. While this simple picture can explain why the actual magnitudes of the velocities are large near the remnant's edge, it is still puzzling why we do not see a smooth trend toward zero velocity, due to projection effects. Our results seem to indicate that some process induces transverse motions, in addition to the purely radial ones.

The various high velocity components seen in IC 2395 show no spatial correlations on distance scales of about 5′, which corresponds to slightly less than a parsec at a distance of 500 pc. This sets a representative upper limit on the sizes of the shocked clouds. For one particular direction, that toward HD 72127A and B, the Ca II data of Hobbs, Wallerstein, and Hu (1982) show that on the distance scale of 3000 AU there is a substantial difference in the structure of the interstellar lines, which had already been noted by Thackeray (1974).

Finally, we examined ESO-SRC Schmidt photographs taken through narrow-band filters centered on Hα and [O III] λ5007, and we found no indication that the presence of filaments near the lines of sight had any influence on the chances of seeing high-velocity absorption lines.

d) Fine-Structure Excitation in Ionized Gases at High Velocities

Only for very few clouds can we calculate useful column density ratios of high-velocity gas in the ground and excited fine-structure states. In the -65 km s^{-1} component of HD 74194, λ1335 of C II* is measurable, giving $\log (W_\lambda/\lambda) = -3.67$. The high velocity component of C II at 1334 Å is blended with the low-velocity component, so we compare it with the S II λ1259 high-velocity component whose $\log (W_\lambda/\lambda) = -4.39$. Since S II and C II are similarly undepleted elements, we assume that their ratio is given by $\log N_S - \log N_C = 1.36$, as in the Sun. The velocity dispersion b of the lines must be limited to less than about 20 km s^{-1};

otherwise, the lines would be noticeably broadened. We then found a lower limit for log (C II*/C II) of -0.9 for $b = 20$ km s^{-1}, rising to the LTE value of $+0.3$ for b at 10 km s^{-1}. Using the information in Table 1 of Spitzer and Jenkins (1975), we find that the C II*/C II ratio restricts the electron density to $\log (n_e T^{-0.5}) > -1.2$. This limit is similar to the data for high velocity clouds found by JSW.

For HD 75821 we have found λ1264 of Si II* to be present and hence can improve the JSW data, since the conclusions in that work were based on the absence of λ1024 of Si II*, which has a small f-value. Our column density for Si II* from the λ1264 line with $\log (W_\lambda/\lambda) = -4.70$ is $10^{12.40}$ cm^{-2} in the cloud at $v = -90$ km s^{-1}. From the λ1526 line of Si II, whose $\log (W_\lambda/\lambda) = -4.38$, we find $\log N(\text{Si II}) = 13.7$. Thus $\log [N(\text{Si II*})/N(\text{Si II})] = -1.3$. This leads to $\log (n_e T^{-0.5})$ of 0.1 [or in the notation of JSW, $\log (n_e T_4{}^{-0.5}) = 2.1$], which is consistent with their fine-structure population analysis for N II which gave $\log (n_e T_4{}^{-0.5}) = +1.6$, but which disagrees with their value of >2.7 from a corresponding treatment for C II. Hence we conclude once again that Si II* and N II* are formed under similar conditions, which differ from the conditions of formation of C II* (JSW, § III*d*).

III. DEPLETIONS

a) Depletion in High-Velocity Clouds

For the high-velocity clouds in front of two stars in the Vela remnant region JSW found that the depletion of nonvolatile species from the gas phase was substantially reduced, probably due to grain evaporation after shocking. For several of the high-velocity clouds detected in this study we can derive the column density ratios of several ionized species. These ratios probably represent total abundance ratios since the second ionization potentials of the elements in question, Al, Si, and Fe, are similar (although that of S is somewhat higher). In the high-velocity clouds the lines are sufficiently weak so as not to be greatly affected by the choice of the velocity dispersion parameter. We have used $b = 12$ km s^{-1} on the basis of the analysis of high-velocity clouds by JSW except for the HD 75821 cloud at -90 km s^{-1}. In this case, the λ1260 and λ1526 lines of Si II indicated that $b = 20$ km s^{-1}.

For comparison, we have analyzed the same ions in low-velocity clouds in front of five stars with lines which were sufficiently weak to be not badly affected by saturation. Three of the stars lie at the smallest distances in Table 1, and the other two are at distances comparable to the remnant but appear outside it. These five stars show the weakest low-velocity lines of all stars in Table 1. For four of the stars we used $b = 12$ km s^{-1}, but for HD 71459 the S II lines indicated a larger b value so we used $b = 20$ km s^{-1}. The derived column densities and their ratios are shown in Table 2.

Mean ratios for the high-velocity clouds and the low-velocity comparison clouds are compared with the ratios of the respective ionic column densities in ζ Oph (Morton 1975) and total abundances in the Sun. (If all ionization stages are used for ζ Oph, the conclusions remain unchanged.) It is clear that the depletions of Al, Si, and Fe, which are large in ζ Oph, are substantially smaller in the high-velocity clouds as compared with the clouds of low velocity. Both HD 74455 and HD 75821 were studied by JSW, but they had no data on Al II. Table 2 indicates that aluminum is strongly depleted in the low-velocity clouds, but that there is more than an order of magnitude less depletion in the high-velocity clouds.

In the high-velocity clouds there can be appreciable concentrations of elements in multiply ionized stages. For example, toward HD 74455, JSW found $\log N(\text{Fe III}) = 13.87$, while $\log N(\text{Fe II}) = 13.14$. We note, however, that the second ionization potential of S, the element with the least depletion under normal circumstances, is higher than those of Al, Si, and Fe. Hence, the ratios of these elements to S are probably higher than the respective ratios of their singly ionized counterparts shown in Table 2. The fact that S is less likely to be ionized more than the other elements is confirmed by the column densities for the -180 km s^{-1} component toward HD 74455 (JSW).

By comparing the equivalent widths of certain interstellar absorption lines in stars observed by *IUE* at high and low galactic latitudes, Jenkins (1983*a*) concluded that the relative

TABLE 2

COLUMN DENSITIES OF IONS SENSITIVE TO DEPLETION IN FIVE HIGH-VELOCITY CLOUDS AND FIVE COMPARISON CLOUDS

		Log N (cm^{-2})				Log of Column Density Ratios			
Star (HD)	V (km s^{-1})	Al II	Si II	S II	Fe II	Al II/S II	Si II/S II	Fe II/S II	Al II/Si II
72089	+93	12.95	13.7	14.4	13.7	−1.45	−0.7	−0.7	−0.75
74194	−65	13.3	...	14.5	13.6	−1.2	...	−0.9	...
74234	+64	12.0	13.2	...	...	...	...	...	−1.2
74455	−175	12.4	13.3	13.6[a]	13.1[a]	−1.2	−0.3	−0.5	−0.9
75821	−90	12.9	13.5	<13.9[a]	14.05[a]	>−1.0	>−0.4	>0.15	−0.6
Mean of high-velocity clouds:						>−1.2	>−0.5	>−0.55	−0.85
63578	+5	13.6	15.0	15.55	14.2	−1.95	−0.55	−1.35	−1.4
69404	+10	13.1	15.0	15.7	14.3	−2.6	−0.7	−1.4	−1.9
71459	+14	13.3	14.3	15.1	14.1	−1.8	−0.8	−1.0	−1.0
72232	+8	13.05	14.95	15.45	14.1	−2.4	−0.5	−1.35	−1.9
76161	−5	13.0	14.6	15.3	14.25	−2.3	−0.7	−1.05	−1.6
Mean of low-velocity clouds:						−2.2	−0.65	−1.20	−1.55
Ratios in ζ Oph:						−3.8	−1.0	−1.5	−2.8
Ratios in solar atmosphere:						−0.8	+0.35	+0.2	−1.15

[a] From *Copernicus* data, revised using f-values of Shull *et al.* 1983.

abundance of iron in the gas phase is enhanced with increasing distance z from the plane. These results primarily reflect the behavior of moderately stirred up gas (i.e., with a radial velocity of a few tens of km s^{-1}), because the lines are strongly saturated. Increases in the relative abundance of Fe II at high z have also been observed by Savage and Bohlin (1979) and Phillips, Gondhalekar, and Pettini (1982). The trends of the abundance ratios with z seem to differ from the behavior we see here for high-velocity gas in the Vela remnant. Jenkins found that $\log [N(\text{Al II})/N(\text{Si II})]$ did not seem to change appreciably from the value -1.2 as z of the target stars increased beyond about 500 pc, while $\log [N(\text{Fe II})/N(\text{S II})]$ crossed from well below the value -0.9 to well above it. By contrast, the high-velocity features toward HD 72089 and HD 74455, both of which show $\log [N(\text{Fe II})/N(\text{S II})] > -0.9$, seem to exhibit a substantial increase in the ratio of Al II to Si II. This also seems to be true for HD 75821, but here one could argue that the lack of Fe depletion is so extreme that a comparison with the high z gas is not appropriate.

The differences between our results and those shown by Jenkins are intriguing, since they suggest that the change in the iron abundance at high z may not be due to the more frequent passage of shocks through the lower density gas. Instead, the iron could be enhanced by some other means, such as enrichment by ejecta from Type I supernovae (Chevalier 1981; Arnett 1982; Wu *et al.* 1983). If this were the case, one could define an upper limit for the ratio of the recycling rate of gas between the disk and halo versus the rate of Fe injection in the halo. We must emphasize, however, that the difference in the abundance patterns we are discussing are far from conclusive. First, we need more good quality observations for high-velocity gas near supernova remnants to substantiate the patterns of reduced depletion. The cases in Table 2 are meager in number. Secondly, one could argue that the apparent lack of change in the Al II to Si II ratio at large z is illusory, since the 1670 Å Al II and 1304 Å Si II lines are quite strong, probably more saturated than the Fe II and S II lines at 1608 and 1253 Å. If the former two lines are on much flatter portions of the curve of growth, the sensitivity to changes in abundance would be much lower. Finally, we should not lose sight of the possibility that the differences could be attributable to shifts in the ionization equilibria of the respective elements.

b) *The Absence of High-Velocity* Al III

Aluminum is the only element which shows lines from its doubly ionized form in our spectra.[2] Al III is never definitely present in the high-velocity gas despite the high transition probabilities of the resonance lines. We can set limits on the ratios of column density of Al III to Si III and Fe III using data published by JSW for HD 74455 and HD 75821. Unfortunately high-velocity S III was not resolved in either star. From an examination of the *IUE* spectra near 1854 Å, we find a safe upper limit for the strongest Al III lines for both stars of $\log (W_\lambda/\lambda)$ at -4.70. For HD 74455 a line may be present at $\log (W_\lambda/\lambda) = -4.85$, i.e., about two-thirds of the strength of our "safe upper limit." The derived ratios of $\log N(\text{Al III})/N(\text{Si III})$ and $\log N(\text{Al III})/N(\text{Fe III})$ are shown in Table 3. A b-value of 12 km s^{-1} was used throughout; only for Si III does the b-value affect the column density (see JSW, Tables 5 and 7).

There are indications from Table 3, especially by comparing Al III/Fe III with Al II/Fe II in HD 74455 that the amount of Al III is very much lower than expected. This is probably due to nonequilibrium ionization and the short recombination time as noted by JSW (Table 19).

IV. C I FINE-STRUCTURE LINES

The presence of absorption lines arising from the excited fine-structure levels of C I[3] allows us to estimate the physical conditions within the clouds where these levels are populated (Jenkins and Shaya 1979). On the basis of a quick look at the data in the first observing session of this survey, JSWL recognized that one star, HD 72350, showed extraordinarily strong absorption lines from the excited levels. These lines indicated that the C I resides in a cloud at an unusually high pressure and that the material had been recently subjected to a shock produced by the supernova blast wave. During our observing run in 1981 June, we observed another star, HD 72648, which also showed strong absorption lines from all three fine-structure levels of C I. These lines appeared to be even stronger than those of HD 72350. A special analysis of the C I lines toward HD 72358 and an interpretation of the conditions toward this star are given in Appendix C.

In this section, we will investigate whether or not the unusually strong excitation of C I is a general phenomenon in the Vela region, if we exclude the two conspicuous cases discussed above. We will compare our results with those obtained from *Copernicus* observations by Jenkins and Shaya (1979) and Jenkins, Jura, and Loewenstein (1983) for stars distributed randomly about the sky.

Unfortunately, when the strengths of the C I lines become weaker than those in the spectra of HD 72350 or HD 72648, noise in the recorded data make the column densities inferred

[2] The λ1206 line of Si III is sometimes visible on our spectra, but the signal-to-noise ratio is usually poor because of the short wavelength and the depression of the continuum by strong stellar lines, even in rapidly rotating B stars.

[3] In this section and Appendices B and C where we differentiate between different levels of excitation, we refer to the unexcited $J = 0$ level as just C I, while C I in the excited $J = 1$ and $J = 2$ states are called C I* and C I**, respectively.

TABLE 3

COMPARISON OF ALUMINUM, SILICON, AND IRON ABUNDANCES IN HIGH-VELOCITY CLOUDS

Star and Component	Al III / Si III	Al II / Si II	Al / Si	Al III / Fe III	Al II / Fe II	Al / Fe
HD 74455; $v = -175$ km s^{-1}	< -1.0	-0.9	-1.0 to -1.3	< -1.5	-0.35	-1.2 to -1.5
HD 75821; $v = -90$ km s^{-1}	< -0.6	-0.8	-0.7 to -0.8	< -1.1	-1.15	-1.2 to -1.3
ζ Oph (low-velocity)	...	...	-2.8	...	...	-2.3
Sun	...	...	-1.15	...	...	-1.0

TABLE 4

WEIGHTED AVERAGES OF C I LINE EQUIVALENT WIDTHS

ABSORPTION-LINE WAVELENGTH (Å)	LINE STRENGTH [log ($f\lambda$)]	FINE-STRUCTURE LEVEL (J)	EQUIVALENT WIDTHS (mÅ)	
			All Stars	Subset Well Outside X-Ray Emitting Region
1328.83	2.04	0	58 ± 6	31 ± 7
1329.10(b)	2.04	1	45 ± 5	15 ± 7
1329.59(b)	2.04	2	27 ± 3	3 ± 6
1560.31	2.34	0	102 ± 11	57 ± 10
1560.69(b)	2.34	1	114 ± 12	45 ± 9
1561.39(b)	2.34	2	68 ± 7	36 ± 10
1656.27	1.97	1	66 ± 7	−8 ± 9

NOTE.—(b) indicates the feature is an unresolved blend of several lines from the same level.

from only one or two exposures of individual stars insufficiently reliable for deriving useful ratios for the excited to unexcited populations. For this reason, we elected to combine the data and interpret the composite results, as outlined below, for all of our stars. This consolidation of the information occurs at the level where equivalent widths are derived, rather than after ratios have been used to deduce gas pressures. The reason for this choice is that the conversion to pressures is a highly nonlinear process, and the end result is far removed from the regime where it is valid to suppress the noise.

For our global measurement of C I populations, we included all stars in the survey (see Table 1 or Fig. 2) except HD 72350 and HD 72648 (the two strong C I cases), and also the following stars which would dilute our result: HD 72232 and HD 76161 which are unquestionably in front of the remnant and HD 63578 which is very far off in the sky. For each star we measured the equivalent widths of selected absorption lines, listed in Table 4, from each of the three fine-structure levels. We then averaged over all stars the equivalent widths in each line. These particular features were favored over other C I transitions covered by the *IUE* wavelength range because absorptions from the different levels are cleanly separated from each other, and they are reasonably strong. Some of the features from a given level consist of two or more lines tightly bunched together in wavelength, however.

Errors σ_i due to noise in each line profile were evaluated from the observed fluctuations in the continuum at nearby wavelengths; they varied significantly from one exposure to another. When individual equivalent width measurements were incorporated into the means, they were weighted by their respective σ_i^{-2}. After deriving a formal error for the weighted means, i.e., $(\Sigma\sigma_i^{-2})^{-1/2}$, we added in quadrature an estimated systematic error equal to 10% of the average equivalent width, to allow for the additional uncertainties due to what we perceived to be a lack of consistent fidelity in deriving the profile intensities. These combined errors were used to define our uncertainties in the final derivations of the three C I column densities. Table 4 lists the weighted mean equivalent widths and their errors.

Without the weighting factors, the mean equivalent widths, when multiplied by the number of stars observed, represent the effect of a single observation over all of the paths to the stars placed end to end, with the absorptions toward each star spaced far enough apart in velocity so that they do not overlap. If all of these absorptions had Gaussian profiles with the same central optical depth and velocity dispersion, a derivation of the net column density using the standard curve-of-growth analysis would give a correct result. In reality, however, the lines of sight probably have significant dispersions in the effective values of these two parameters. Even so, Jenkins (1983*b*) has shown that the effect of such dispersions, even when they are not small compared to the respective averages, give a resultant curve of growth which differs little from the shape of a curve corresponding to one with the overall mean value of central optical depth and velocity width.

For each of the three excitation levels of C I, we derived the χ^2 values for various combinations of column density N and velocity dispersion b to obtain reasonable confidence limits (95%) for the allowed values. Table 5 lists the resultant column densities for three representative values of b. Some of the absorption features from the excited levels are actually blends of two or more lines which are unresolved. We calculated the expected widths for these composite features using modified curves of growth which were based on explicit calculations of the structure of the overlapping components. Uncertainties in the f-values for the transitions were not included in the estimates for the error budget of N and b.

If one were to assume that the three levels collectively have the same value of b, then the range for b is restricted to 8–32 km s^{-1} ($b > 32$ km s^{-1} would produce significantly broader lines than those observed). While this assumption may seem to be reasonable, we note that a few, isolated counter-examples showing mild discrepancies in b have been found from the *Copernicus* C I surveys (Jenkins, Jura, and Loewenstein 1983).

To derive information on the distribution of gas pressures along the observed lines of sight, we repeated the geometric method of interpretation devised by Jenkins and Shaya (1979). Figure 3 shows areas which contain the allowed combinations

TABLE 5

COMPOSITE COLUMN DENSITIES OF C I IN VELA SNR

FINE-STRUCTURE LEVEL (J)	LOG COLUMN DENSITIES (cm^{-2})		
	$b = 5$ km s^{-1}	$b = 8$ km s^{-1}	$b = 32$ km s^{-1}
0	13.95–14.50	13.70–14.00	13.55–13.70
1	not allowed	13.65–13.75	13.50–13.65
2	13.35–13.60	13.30–13.50	13.25–13.45

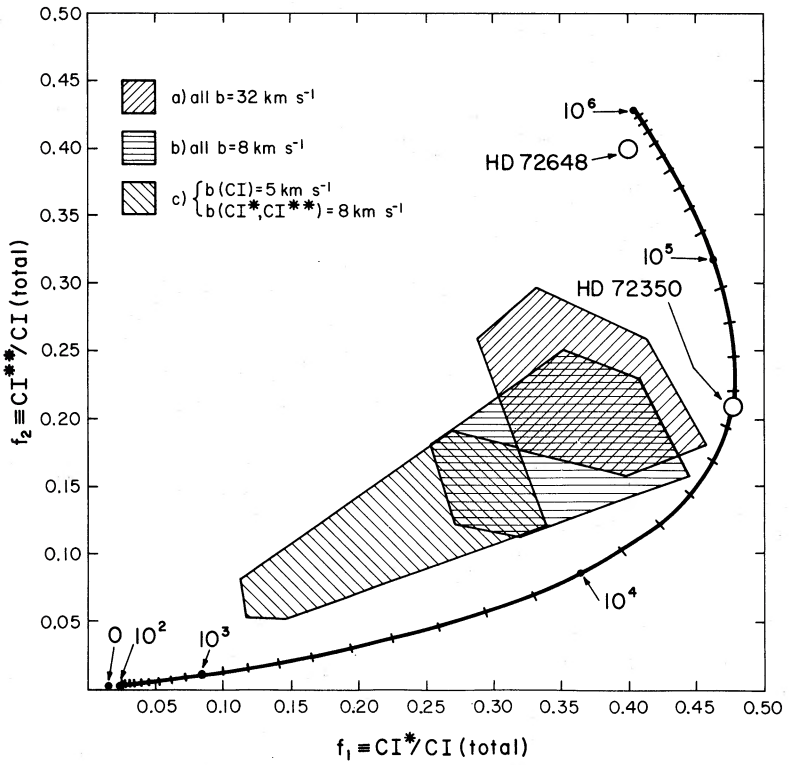

FIG. 3.—Allowed possibilities for the fraction of neutral carbon in either of the two fine-structure levels. Except for HD 72648 and HD 72350 which had extraordinarily strong C I lines and are shown separately here, the data from all of our stars were averaged together, and the error boxes for the population ratios are shown for three possibilities for the net velocity dispersion of the lines. The family of points along a curve show the expected ratios for homogeneous regions at a temperature of 100 K and at various pressures (with the pressures p/k of some points being indicated in terms of cm^{-3} K).

of f_1 [$\equiv N(\text{C I}^*)/N(\text{C I}_{\text{total}})$] and f_2 [$\equiv N(\text{C I}^{**})/N(\text{C I}_{\text{total}})$] for all possible combinations of N inside the limits given in Table 5 if (*a*) the b values for all three levels are identical and have the value 32 km s^{-1}, (*b*) same as (*a*) except $b = 8$ km s^{-1}, and (*c*) the b of the two excited levels equals 8 km s^{-1} but there is extra material at a low-velocity dispersion which is principally unexcited and gives an effective $b = 5$ km s^{-1} for the $J = 0$ column density. Also shown are the most probable f_1 and f_2 values for HD 72350 and HD 72648.

For a temperature of 100 K, the curve plotted on the diagram shows the locus of points expected for homogeneous regions at different pressures. As discussed by Jenkins and Shaya (1979), a composite measurement of many separate C I–bearing regions will produce an apparent f_1 and f_2 which is positioned at the "center of gravity" of points lying on the equilibrium curve for each region, with the weight of each point being proportional to the respective value of $N(\text{C I}_{\text{total}})$. One cannot arrive at a unique interpretation for the distribution of C I at different pressures, but instructive examples can be devised from the composite f_1 and f_2 values. For instance, for cases (*a*) and (*b*) discussed above, the results are consistent with 20%–70% of the C I being at a pressure above 10^5 cm^{-3} K and the remainder at, or slightly below, a pressure of $10^{3.8}$ cm^{-3} K. Another alternative is that all of the gas is at a pressure between 10^4 and 10^5 cm^{-3} K, and the mean pressure is around $10^{4.4}$ cm^{-3} K. If case (*c*) is closer to reality, one would surmise that there are large contrasts in pressure from place to place, but the fraction of C I above 10^5 cm^{-3} K could be as little as 10%.

From the standpoint of the distribution of H I gas pressures, one must remember that the fraction of carbon in un-ionized form scales linearly with pressure. The time constant for readjusting the ionization equilibrium of carbon is from one to several hundred years. Thus, for all but very recently shocked clouds, the C I results tend to emphasize the higher pressure gas, and one must compensate for this effect.

With even a conservative interpretation of the C I populations (i.e., case [*c*]), the Vela stars show significantly more high pressure gas than the fraction seen toward stars in the general *Copernicus* surveys of interstellar C I (Jenkins, Jura, and Loewenstein 1983). In these surveys, with a cumulative coverage of 20 kpc in various directions, the amount of C I at pressures above 10^5 cm^{-3} K is of order 1% of the total. Most of the H I gas in the general interstellar medium seemed to have nT between 10^3 and 10^4 cm^{-3} K.

As discussed in § II*b*, five stars are well outside the X-ray emitting region of the remnant (HD 69404, HD 69973, HD 70309, HD 70930, and HD 74753). To see if there was any evidence that increased pressures could be found beyond the X-ray edges (or where we see high-velocity gas), we measured this subset of five stars separately (the subset *was* included in the grand total, however). The last column of Table 4 lists the weighted averages and errors for the absorption-line equivalent widths of just these stars. These results strongly suggest that the populations of the excited levels are lower than for our complete sample. Unfortunately, we cannot assert this unequivocally, because the uncertainty of N and b for the five stars

is large enough to permit an overlap with the general population ratios, if one considers the worst possible extremes in each case.

The high pressures associated with the Vela supernova remnant come as no surprise. Quantitatively, the observations agree well with models of a remnant assumed to be in the adiabatic phase, which overtakes and compresses ambient interstellar clumps or filaments. For instance, we may look at a simple interpretation of the Sedov-Taylor solution where the average pressure $\langle p \rangle$ within a remnant of radius R is two-thirds of the thermal energy density

$$\langle p \rangle = \frac{2}{3}\frac{3E_{\rm th}}{4\pi R^3}$$

and the immediate postshock pressure $p_1 = 2.13\langle p \rangle$ (Ostriker and McKee 1983) if $\gamma = 5/3$ and the interior density equals that on the outside (i.e., there is no addition of material to the intercloud matrix inside the remnant from cloud evaporation). We may integrate the growth of the remnant's outer boundary

$$v_B = (4p_1/3\rho_0)^{1/2}$$

to obtain R as a function of $E_{\rm th}$, the age of the remnant t and the ambient intercloud number density ρ_0

$$R = \left[\frac{25}{6\pi}\right]^{1/5}\left(\frac{2.13\ E_{\rm th}}{\rho_0}\right)^{1/5} t^{2/5}\ .$$

If we solve for $\langle p \rangle/k$ and express $E_{\rm th}$, the ambient density n_0, and remnant age t in terms of units close to the conditions in the Vela remnant, 5×10^{50} ergs, 0.1 cm^{-3}, and 1.8×10^4 yr, respectively, we obtain

$$\langle p \rangle/k = 10^{6.17} E_{\rm th}^{2/5} n_0^{3/5} t^{-6/5}\ {\rm cm}^{-3}\ {\rm K}\ .$$

If, instead of the classical Sedov-Taylor solution, we consider McKee and Ostriker's (1977) description of a remnant's evolution dominated by cloud evaporation, we find (with the same units for $E_{\rm th}$ and t)

$$\langle p \rangle/k = 10^{6.76} E_{\rm th}^{7/10} t^{-9/5} \Sigma^{-3/10}\ {\rm cm}^{-3}\ {\rm K}\ ,$$

where the parameter Σ is defined to be a measure of the effectiveness of cloud evaporation in depositing extra mass into the remnant's interior. With reasonable guesses for the properties of the embedded clouds, one infers that $\log \Sigma$ could range from about -1 to $+2$. Whether or not the Vela remnant is in the evaporation-dominated regime is not very clear, since the quantity

$$x = 0.43 R_{20} \Sigma^{1/5} n_0^{3/5} E_{\rm th}^{-2/5}\ ,$$

which parameterizes the density excess due to evaporated gas and is defined in McKee and Ostriker's equation (6), is not very different from unity (R_{20} is the remnant's radius in units of 20 pc; we calculate a radius of 22 pc for the Vela remnant if its distance is 500 pc and the apparent diameter of its X-ray emission is 5°—this radius is consistent with the radius one obtains in the pure Sedov-Taylor case using the numerical values for $E_{\rm th}$, n_0, and t given above). In either case, however, it is clear that pressures substantially more than 10^6 cm^{-3} K should prevail within the Vela remnant.

As emphasized by Jenkins, Jura, and Loewenstein (1983), C I-bearing clouds probably do not respond to the external pressure pulses rapidly enough to reflect the full effect of the intercloud pressure rise. In the absence of a magnetic field, an isothermal shock starting from the outer edge of any cloud will propagate at a velocity $\beta = C(\rho_1/\rho_0)^{1/2}$, where ρ_1 and ρ_0 are the pre- and postshock densities, and the speed of sound C in the cloud is $\approx$0.5 km s^{-1}. If $\log p/k$ jumps from 3.5 to 6.5, for example, $\beta \approx 15$ km s^{-1}, and the shock will have covered only the outer 0.15 pc of a cloud in 10^4 yr. Thus clouds having a diameter more than a few pc will have only a small fraction of their C I responding to the pressure rise.

V. HIGHLY IONIZED ATOMS AT LOW VELOCITIES

In § II we showed that the Vela remnant has a generous number of Si IV and C IV features at high velocities. Low-velocity counterparts for these ions were also detected. The reliability of the low-velocity Si IV and C IV measurements was compromised, at times, by the presence of photospheric absorptions by these same ions. On a few occasions we were not sure exactly where to draw the "continuum" for an interstellar line embedded within a stellar one. Also, the stellar troughs lowered the intensity of starlight near the interstellar features which in turn lowered our signal-to-noise ratio. Our misgivings about the reliability of individual measurements are reinforced by our observation that 30% of the cases where the stronger line had $W_\lambda > 50$ mÅ gave a doublet ratio outside the proper range of 1.0 to 2.0.

For the reasons stated above, we are reluctant to regard our low-velocity, highly ionized features from a standpoint other than considering a global average over a substantial collection of lines of sight, as we had done for the weak C I features. Thus, for our analysis of low-velocity, interstellar Si IV, C IV, and N V, we repeated the methods outlined in § IV, except that we increased our estimates of the overall systematic errors to 25% to allow for the uncertainties from the stellar lines. Tables 6 and 7 present our equivalent widths and composite column densities in formats similar to those of Tables 4 and 5. While the total equivalent widths for N V seem to be significant, we could not see convincing interstellar components in any of the single recordings. When measuring the spectra in the vicinity of the N V wavelengths, we were careful not to be influenced by apparent downward fluctuations and only considered velocity intervals defined by the Si IV and C IV features.

For both Si IV and C IV, we found that the most probable b was 15 km s^{-1}. Values of b much larger than 32 km s^{-1} could be ruled out from the apparent narrowness of the lines. With the errors we have estimated for the equivalent widths, the Si IV and C IV doublets could have nearly equal strengths. Hence we cannot rule out the possibility that $b \ll 15$ km s^{-1}, and the respective column densities are arbitrarily large. For N V we are unable to determine b, but the lines are almost certain to be unsaturated.

While the equivalent widths of the Si IV and C IV lines toward stars outside the X-ray emitting region are lower than the overall average, solutions for the most probable column densities are very close to those listed for $b = 15$ km s^{-1} because the apparent doublet ratios are closer to unity. However, we cannot declare that b for the subset is significantly lower than that of the complete sample with the errors that we have defined. There is a hint that N V may be more abundant outside the X-ray boundary, somewhat contrary to expectation, but again the errors are large enough to preclude a definitive conclusion. While it has been pointed out that

TABLE 6

WEIGHTED AVERAGE EQUIVALENT WIDTHS OF FEATURES FROM HIGHLY IONIZED ATOMS AT LOW VELOCITY

Ion	Absorption-Line Wavelengths	Line Strength [log ($f\lambda$)]	Equivalent Widths (mÅ) All Stars	Equivalent Widths (mÅ) Subset Well Outside X-ray Emitting Region
Si IV	1393.76	2.866	158 ± 40	119 ± 31
Si IV	1402.77	2.565	114 ± 29	87 ± 23
C IV	1548.20	2.478	212 ± 53	137 ± 35
C IV	1550.77	2.177	169 ± 42	125 ± 32
N V	1238.82	2.275	24.5 ± 6.6	38.9 ± 12.1
N V	1242.80	1.973	8.8 ± 3.2	13.2 ± 7.1

ionizing radiation from hot target stars can produce significant amounts of Si IV and some C IV along the lines of sight (Black *et al.* 1980), only five out of the 42 stars we considered have an effective temperature greater than the 25,000 K needed to produce measurable Si IV and C IV absorption lines (see Table 1 for spectral types).

The average distance to all of the stars is 870 pc. Thus, the average number densities along all of the lines of sight (taking log N values in the middle of the ranges corresponding to $b = 15$ km s^{-1}) turn out to be 1.3×10^{-8}, 6×10^{-8}, and 3.5×10^{-9} cm^{-3} for Si IV, C IV, and N V, respectively. By comparison, the general interstellar medium near the plane of our galaxy has $\langle n(\text{Si IV})\rangle = 3.6 \times 10^{-9}$ cm^{-3} (Jenkins 1981), $\langle n(\text{C IV})\rangle = 5.5 \times 10^{-9}$ cm^{-3} (Jenkins 1981; Cowie, Taylor, and York 1981), and $\langle n(\text{N V})\rangle = 1\text{–}2 \times 10^{-9}$ cm^{-3} (Jenkins 1981; York 1977). The significant excesses for these ions toward stars in the direction of the Vela remnant are in accord with the large overabundance of O VI recorded by JSW, who concluded that the low-velocity, highly ionized atoms are produced in conductive boundary layers surrounding clouds behind the shock front. We do note, however, that relative to C IV there is too much Si IV (by a factor of 3.5) and too little N V (down by a factor of 7) when we compare our observations with calculations of time-dependent ion fractions within evaporative interfaces (Weaver *et al.* 1977). A similar problem of too much Si IV exists with the general interstellar medium (Jenkins 1981).

There may be a simple way to reconcile the Si IV and N V anomalies. From improved calculations of collisional equilibrium of Shull and Van Steenberg (1982), we note that N V/N = $10^{-1.46}$, C IV/C = $10^{-0.81}$, and Si IV/Si = $10^{-1.82}$ at $T = 10^{5.1}$ K, which means Si IV/C IV = $10^{-2.03}$ and N V/C IV = $10^{-1.16}$ if cosmic abundances prevail. Hence the N V abundance can be understood if the gas is collisionally ionized at $T \sim 10^{5.1}$ K, but even though this temperature is near that where Si IV/Si should reach its maximum value, there is still a problem with there being too much observed Si IV. The resolution of this may be due to the presence of an additional source of ionization by UV radiation from the shocked gas. Models of ionization by precursor radiation in shocks at $v > 100$ km s^{-1} (Shull and McKee 1979) show that Si IV/Si ~ 1. Hence it may be possible to have a self-consistent model of low velocity gas which reconciles our measurements of Si IV, C IV, and N V.

TABLE 7

COMPOSITE COLUMN DENSITIES OF HIGHLY IONIZED ATOMS AT LOW VELOCITY (ALL STARS)

Ion	Log Column Densities (cm^{-2}) $b = 15$ km s^{-1}	Log Column Densities (cm^{-2}) $b = 32$ km s^{-1}
Si IV	13.20–13.85	13.15–13.60
C IV	13.75–14.65	13.65–14.15
N V	12.76–13.20	12.76–13.16

VI. SUMMARY

In summary, the high pressures found within cold clumps inside the Vela supernova remnant confirm the inhomogeneous model of the ambient surrounding interstellar medium that we originally proposed in 1975. The pattern of reduced depletion with increasing component velocity, found here for Al, and confirmed for Si and Fe, is consistent with the model of grain destruction and ablation in supernova shocks. The velocity pattern, enhanced but chaotic within the remnant, and extending out to beyond the region of intense soft X-ray emission, is extremely suggestive of a model in which the remnant evolution is dominated by interactions with pre-existing interstellar clouds.

This research was supported by NASA grants NSG-5248, NSG-5374 and NGR 05-003-578 to Princeton University, the University of Washington, and the University of California, respectively. Additional support came from NASA contract NAS5-23576 to Princeton. The authors are indebted to G. M. Voit for his perseverance in measuring the velocities and equivalent widths of an enormous collection of interstellar line tracings. Mr. Voit also wrote the programs for calculating the curves of growth for those C I lines which were blended. We gratefully acknowledge the assistance of the *IUE* Observatory staff in the acquisition and initial reduction of our spectra.

APPENDIX A

NEW OBSERVATIONS OF Ca II AND Na I

New spectra of several important stars were obtained for us by Drs. E. Hu and N. Walborn at the Ca II and Na I lines. These spectra taken with the CTIO 4 m echelle spectrograph have a dispersion of 2.2 Å mm^{-1} at H and K, and a dispersion of 3.3 Å mm^{-1} at the D lines. They were measured with a small visual measuring engine by G. W. while at Princeton and traced for intensity using the microphotometer at the University of Washington. Radial velocities, equivalent widths, column densities, and velocity parameters are listed in Table 8. Resolved components are differentiated by letters.

In addition to providing useful data to aid in the interpretation of the *IUE* data, the new optical material is interesting in its own right. The six interstellar components in HD 72089 provide a one-star example of the Spitzer-Routly (1952) effect (Siluk and Silk 1974). The lowest velocity component is seen in Na I only. It is flanked by two strong sodium components that are weak in Ca II while three additional components of Ca II with velocities of −77, +72, and +104 km s^{-1} are not present in sodium.

For HD 72350 two low-velocity components of Na I are accompanied by moderately strong Ca II while an additional component of Ca II without any sodium is present at +36 km s^{-1}. The resolution into two low-velocity components clarifies the unusually high Na I column densities reported by WSJ from spectra at 18 Å mm^{-1} because the addition of the two components yields lines that are heavily saturated while the separate components are only moderately saturated. The C I lines in HD 72350 show a radial velocity of +12.3 km s^{-1} which agrees closely with component *b* of sodium at 14.3 km s^{-1} rather than the other component at −2.4 km s^{-1}. Our *IUE* velocity for lines of S II, Si II, and Fe II is +7.7 km s^{-1} which is close to the mean velocity of the two strong Ca II components, viz. 9 km s^{-1}. Hence we see that both Ca II clouds contribute to the ionized gas seen with *IUE*, while the high-density neutral carbon cloud is associated with only one of the sodium features.

APPENDIX B

C I LINES IN INDIVIDUAL STARS

Though we believe that the statistical method of combining C I data for all the program stars provides a preferable method of deriving the global properties of neutral gas in the Vela remnant, the data for individual stars frequently shed some light on the pressures in individual clouds. Since we have only one exposure of most of the stars, these data are very uncertain due to limited signal-to-noise ratios. In addition, the stars have been selected by the criterion that the various

TABLE 8

RADIAL VELOCITIES (WITH RESPECT TO LSR), EQUIVALENT WIDTHS, COLUMN DENSITIES, AND *b*-VALUES FOR OPTICAL LINES

Star	Line	V_r	Log (W_λ/λ)	Line	V_r	Log (W_λ/λ)	Log N (cm^{-2})	b (km s^{-1})
HD 72089	Ka	−76.8	−5.56	Ha	...	−5.98	11.05	...
	Kb	−13.4	−5.28	Hb[a]	...	...	11.35	...
	Kc	...	< −5.6	Hc[a]	...	...	< 11.0	...
	Kd	+12.5	−5.04	Hd[a]	...	...	11.65	> 2[b]
	Ke	+72.1	−4.63	He	...	−4.84	12.2	> 2
	Kf	+104.0	−5.03	Hf	...	−5.24	11.7	> 1.5
HD 72089	D2a	...	< −5.6	D1a	...	< −5.6	< 11.0	...
	D2b	−15.7	−4.63	D1b	−18.2	−4.90	12.0	> 2
	D2c	−1.9	−4.8[c]	D1c	...	−5.1[c]	11.8	...
	D2d	+13.8	−4.90	D1d	+10.8	−5.21	11.7	> 2
	D2e	...	< −5.6	D1e	...	...	< 11.0	...
	D2f	...	< −5.6	D1f	...	...	< 11.0	...
HD 72350	Ka	+1.3	−4.54	Ha[a]	...	...	12.3	> 3[b]
	Kb	+16.6	−4.46	Hb	...	−4.78	12.3	≥ 4
	Kc	+35.7	−5.03	Hc	...	−5.30	11.65	...
HD 72350	D2a	−2.4	−4.33	D1a	−4.0	−4.42	12.7	≥ 4
	D2b	+14.3	−4.37	D1b	+12.8	−4.42	≥ 12.8	≤ 4
	D2c	...	< −5.6	D1c	...	< −5.6	< 11.0	...
HD 74234	Ka	−6.4	−5.30	Ha	...	−5.33	11.45	...
	Kb	+2.8	−4.34	Hb	...	−4.65	12.4	≥ 8
HD 74920	Ka	−18.6[d]	...	Ha	...	...	...	...
	Kb	+2.0	−4.99	Hb	...	−5.01	11.85	...
	Kc	+57.8[d]	...	Hc	...	...	...	...

[a] Strongly affected by blending with stellar Hε.
[b] Assumed.
[c] Very uncertain due to blending.
[d] Presence is uncertain.

TABLE 9

C I COLUMN DENSITIES AND THEIR RATIOS FOR INDIVIDUAL STARS IN THE DIRECTION OF THE VELA REMNANT

Star (HD)	Lowest b-Value (km s^{-1})	C I	C I*	C II**	f_1	f_2	Highest b-Value (km s^{-1})	C I	C I*	C I**	f_1	f_2
63578	5	13.9	13.9	13.1:	0.49	0.08:	20	13.45	13.65	13.0	0.54	0.12:
72798	13	13.95	14.0	13.85	0.37	0.28	25	13.8	13.85	13.75	0.37	0.30
74234	5	13.95	13.85	13.3	0.40	0.10	10	13.7	13.7	13.15	0.42	0.13
74251	13	14.05	13.8	13.65	0.30	0.20	40	13.85	13.75	13.6	0.34	0.23
74530	10	14.15	13.9	13.35	0.31	0.09	25	13.9	13.75	13.3	0.38	0.12
74580	8	>13.75	14.2	13.8	<0.56	<0.22	25	13.8	13.85	13.75	0.38	0.30

lines of C I, C I*, and C I** yield reasonably consistent results. This means that we have included only stars whose equivalent widths had smaller than average random errors and hence whose column densities as derived from several multiplets look more consistent than those based upon equivalent widths with larger random errors. We believe, but cannot be certain, that this selection should not affect the resulting column density ratios, f_1 and f_2, in a systematic way.

Column densities for the highest and lowest acceptable b-values and column density ratios are shown in Table 9. For all of the stars except HD 72648 the lines are sufficiently weak that the column densities are not greatly affected by the b-values. Hence the column density ratios f_1 and f_2 discussed earlier are virtually unaffected by the choice of b-value, and the b-value is not well determined.

Since the f_1 and f_2 ratios given in the table do not define uniquely both the kinetic temperature and pressure, it is probably more instructive to compare them with field stars (Jenkins and Shaya 1979) and show qualitatively that the physical conditions for neutral gases in front of the Vela stars are truly atypical. Four of the stars lie above and to the right, in the f_1-f_2 diagram, of any of the stars in the Jenkins and Shaya survey. In fact, these four stars have values of f_1 and f_2 which are similar to those of HD 72350 for which JSWL found $p/k > 10^{4.2}$ cm^{-3} K, and three of them have much lower column densities of C I than that of HD 72350. For all four stars we can say with considerable confidence that $T > 30$ K and that $p/k \geq 10^5$.

APPENDIX C

The star HD 72648 shows the strongest C I, C I*, and C I** lines of any star in this program and, as far as we know, any other program for which *IUE* or *Copernicus* data have been published. We have detected in the spectrum of this star even the very weak lines at 1276.48, 1276.75, and 1280.85 Å, lines which are not visible toward another star, HD 72350, whose spectrum we had previously identified as having unusually strong C I lines in the different stages of excitation (JSWL). In this Appendix we derive the physical properties of the absorbing cloud, as we did for HD 72350. Table 10 lists the equivalent widths of the lines that we have used. These determinations are not as accurate as those for HD 72350 because we have only one exposure rather than three.

We derived C I column densities only from the weakest lines (mentioned above) and obtained $10^{14.7}$, $10^{14.8}$, and $10^{14.8}$ cm^{-2} for C I, C I*, and C I**, respectively [giving $\log N(\text{C I}_{\text{total}}) = 15.2$]. The strong lines are not useful for determining the column density but tell us that $b = 13$ km s^{-1}, a reasonable value. The column density ratios f_1 and f_2, as defined by Jenkins and Shaya (1979), are both equal to about 0.36, which places this cloud in their Figure 6 near $\log T = 2$ and $\log p/k = 6$.

The physical conditions in the neutral cloud can be evaluated further with the help of the O I* and O I** column densities, both of which are $10^{14.1}$ cm^{-2} from the equivalent widths in Table 10 and the b value derived from C I. From this determination that $\log [N(\text{O I**})/N(\text{O I*})] = 0.0 \pm 0.1$, the limits on the kinetic temperature are $2.25 < \log T < 3.25$, irrespective of pressure. The upper limit is almost indefinite if the uncertainty is any larger because the population ratio approaches the ratio of statistical weights. At the other extreme, an error of 0.3 in the logarithmic abundance ratio still leaves $\log T > 2.0$.

We could further restrict the kinetic temperature if we had a figure for the column density of unexcited O I in the dense region. Unfortunately, the O I line at 1302.169 Å is so strong that it must be far out on the flat portion of the curve of growth, which makes N(O I) virtually indeterminate, even if we know the appropriate b value. Furthermore, along the line of sight much of the O I in the zero-volt fine-structure level may be outside the region represented by the C I. This is because C I, unlike O I, is in a lower stage of ionization than the most abundant one for H I regions, so it emphasizes clouds which have a higher density of electrons. However, for the C I-bearing regions we can estimate the amount of unexcited O I indirectly. We begin by calculating the abundance of C II by scaling upwards the observed amount of C I using the equation for the C I–C II ionization equilibrium. In this calculation, we assume that carbon atoms are not appreciably depleted (Jenkins, Jura, and Loewenstein 1983) and that nearly all of the free electrons come from the photoionization of carbon by the general interstellar radiation field (see eq. [12] of Jenkins and Shaya 1979). The fact that HD 72648 lies 700–800 pc behind the Vela remnant assures us that if the C I cloud is in the remnant, its ionization is not affected by the radiation field of HD 72648. To arrive at an estimate for N(O I), we assume the ratio of oxygen to carbon in the dense cloud is not much different from the cosmic abundance ratio. Because of its dependence on the carbon ionization equilibrium, the inferred abundance of O I

TABLE 10

EQUIVALENT WIDTHS OF INTERSTELLAR LINES IN FRONT OF HD 72648

λ (Å)	Identification	Log $f\lambda$	Log (W_λ/λ)
1261.52	C I**	1.68	−3.80
1276.48	C I	0.80	−4.52
1276.75	C I*	0.80	−4.48
1280.85	C I**	0.95	−4.35
1302.17	O I	1.80	−3.61
1304.86	O I*	1.80	−4.15
1306.03	O I**	1.80	−4.10
1328.83	C I	2.04	−3.92
1329.10	C I*	2.04	−3.96
1329.59	C I**	2.04	−3.94
1447	CO(3–0)	1.56	−3.99
1477	CO(2–0)	1.66	−3.91
1509	CO(1–0)	1.62	−3.68
1544	CO(0–0)	1.34	< −4.7
1560.31	C I	2.10	−3.80
1560.69	C I*	2.13	−3.82
1561.39	C I**	2.10	−3.73
1656.27	C I*	1.97	−3.86
1657.38	C I*	1.75	−4.10

is inversely proportional to the assumed pressure, to a good approximation, and varies as $T^{1.6}$.

An interesting conclusion arises from our calculation of N(O I) outlined above. Regardless of the assumed pressure, we find that the observed N(O I*) divided by the inferred N(O I) is less than the relative population of O I in the first excited level that we calculate for collisional equilibrium with neutral hydrogen atoms. For log $T = 2.25$, the discrepancy is about a factor of 2.3, which is not too bad considering the uncertainties in many of our assumptions. The difference widens for higher temperatures, reaching a factor of about 26 when log T approaches 3.0. Thus, our indirect determination of N(O I) indicates that the actual temperature in the highly compressed region is probably not much greater than our lower limit indicated from the ratio of N(O I**)/N(O I*), log $T = 2.25$.

We note that the observed reddening $E(B-V)$ of HD 72648 is 0.38 (Eggen 1982). This, combined with the empirical relationship $N(\text{H I})/E(B-V) = 5.8 \times 10^{21}$ cm^{-2} mag^{-1} (Bohlin, Savage, and Drake 1978), gives a value of $10^{21.3}$ cm^{-2} for N(H I). This is an upper limit to N(H I) in the high-pressure cloud, since some of the reddening and H I are undoubtedly due to material elsewhere along the 1200 pc line of sight. If we go back to our calculation of the C II–C I ionization equilibrium (and again assume a cosmic C to H abundance ratio), we find for log $T = 2.25$ that log p/k must be greater than 4.5 to avoid violating our upper limit for N(H) derived from the reddening. Thus we have independent confirmation that the pressure in the cloud is far above the average for the interstellar medium. Quantitatively, however, this conclusion is not as forceful as what we found from the fine-structure population ratios.

In summary, the line of sight toward HD 72648 has a parcel of gas which is very dense, with n certainly greater than 10^3 cm^{-3} and probably even above 10^4 cm^{-3}. The temperature of this region, however, is not appreciably different from that found in normal, diffuse, interstellar clouds. These conditions suggest that we may be dealing with shock compression of a preexisting cloud after the passage of the supernova shock wave. As discussed by JSWL, such compression may lead to star formation. In connection with this possibility, we can compare the column density of C I with that of CO to see if this region is a molecular cloud. From the data of Table 10, we find log $N(\text{CO}) = 14.4 \pm 0.2$, provided that we can assign log $W_\lambda/\lambda = -4.7$ to the 0–0 feature that we were unable to detect. Hence, log C I/CO = 0.7, or one-sixth of the carbon is in CO. This is consistent with what is seen in unpressurized diffuse clouds in general (Federman *et al.* 1980) and is similar to the ratio seen in the cloud in front of HD 72350 (JSWL).

REFERENCES

Arnett, W. D. 1982, *Ap. J.*, **253**, 785.
Black, J. H., Dupree, A. K., Hartmann, L. W., and Raymond, J. C. 1980, *Ap. J.*, **239**, 502.
Bohlin, R. C., Savage, B. D., and Drake, J. F. 1978, *Ap. J.*, **224**, 132.
Chevalier, R. A. 1981, *Ap. J.*, **246**, 267.
Cowie, L. L., Taylor, W., and York, D. G. 1981, *Ap. J.*, **248**, 528.
Culhane, J. L. 1977, in *Supernovae*, ed. D. N. Schramm (Boston: Reidel), p. 29.
Eggen, O. J. 1982, *Ap. J. Suppl.*, **50**, 199.
Federman, S. R., Glassgold, A. E., Jenkins, E. B., and Shaya, E. J. 1980, *Ap. J.*, **242**, 545.
Hipplelein, H. H., and Weinberger, R. 1975, *Astr. Ap.*, **43**, 405.
Hobbs, L. M., Wallerstein, G., and Hu, E. 1982, *Ap. J. (Letters)*, **252**, L17.
Jenkins, E. B. 1981, in *The Universe at Ultraviolet Wavelengths, The First Two Years of International Ultraviolet Explorer*, ed. R. D. Chapman (NASA CP-2171), p. 541.
———. 1983*a*, in *Kinematics, Dynamics and Structure of the Milky Way*, ed. W. L. H. Shuter (Dordrecht: Reidel), p. 21.
———. 1983*b*, in preparation.
Jenkins, E. B., Jura, M. J., and Loewenstein, M. 1983, *Ap. J.*, **270**, 88.
Jenkins, E. B., and Shaya, E. J. 1979, *Ap. J.*, **231**, 55.
Jenkins, E. B., Silk, J., and Wallerstein, G. 1976*a*, *Ap. J. (Suppl.)*, **32**, 681 (JSW).
———. 1976*b*, *Ap. J. (Letters)*, **209**, L87.
Jenkins, E. B., Silk, J., Wallerstein, G., and Leep, E. M. 1981, *Ap. J.*, **248**, 977 (JSWL).
Kahn, S., and Seward, F. 1982, private communication.
Lyngå, G. 1962, *Ark. Astr.*, **3**, 65.
McKee, C. F., Cowie, L. L., and Ostriker, J. P. 1978, *Ap. J. (Letters)*, **219**, L23.
McKee, C. F., and Ostriker, J. P. 1977, *Ap. J.*, **218**, 148.
Morton, D. C. 1975, *Ap. J. (Letters)*, **193**, L35.
Ostriker, J. P., and McKee, C. F. 1983, in preparation.
Phillips, A. P., Gondhalekar, P. M., and Pettini, M. 1982, *M.N.R.A.S.*, **200**, 687.
Reynolds, R. J. 1976, *Ap. J.*, **203**, 151.
Routly, P. M., and Spitzer, L. 1952, *Ap. J.*, **115**, 227.
Savage, B. D., and Bohlin, R. C. 1979, *Ap. J.*, **229**, 136.
Shull, J. M., and McKee, C. F. 1979, *Ap. J.*, **227**, 131.
Shull, J. M., and Van Steenberg, M. 1982, *Ap. J. Suppl.*, **48**, 95.
Shull, J. M., Van Steenberg, M., and Seab, C. G. 1983, *Ap. J.*, **271**, 408.
Siluk, R. S., and Silk, J. 1974, *Ap. J.*, **192**, 51.
Spitzer, L., and Jenkins, E. B. 1975, *Ann. Rev. Astr. Ap.*, **13**, 133.
Thackeray, A. D. 1974, *Observatory*, **94**, 55.
Wallerstein, G., Jenkins, E. B., and Silk, J. 1980, *Ap. J.*, **240**, 834.
Weaver, R., McCray, R., Castor, J., Shapiro, P., and Moore, R. 1977, *Ap. J.*, **218**, 377.
Wu, C., Leventhal, M., Sarazin, C. L., and Gull, T. R. 1983, *Ap. J. (Letters)*, **269**, L5.
York, D. G. 1977, *Ap. J.*, **213**, 43.

EDWARD B. JENKINS: Princeton University Observatory, Princeton, NJ 08544

JOSEPH SILK: Astronomy Department, University of California, Berkeley, CA 94720

GEORGE WALLERSTEIN: Astronomy Department, FM-20, University of Washington, Seattle, WA 98195